Journal of Power Sources 381 (2018) 38–45

Contents lists available at ScienceDirect

Journal of Power Sources

journal homepage: www.elsevier.com/locate/jpowsour

Capacity extended bismuth-antimony cathode for high-performance liquid metal battery

Tao Dai[a], Yue Zhao[a], Xiao-Hui Ning[a,*], R. Lakshmi Narayan[b], Ju Li[c,**], Zhi-wei Shan[a]

[a] Center for Advancing Materials Performance from the Nanoscale (CAMP-Nano), State Key Laboratory for Mechanical Behavior of Materials, Xi'an Jiaotong University, Xi'an 710049, PR China

[b] Department of Materials Science and Engineering, Carnegie Mellon University, Pittsburgh, PA 15213, USA

[c] Department of Nuclear Science and Engineering, and Department of Materials Science and Engineering, Massachusetts Institute of Technology, Cambridge, MA 02139, USA

HIGHLIGHTS

- The electrochemical behavior of Bi-Sb alloy cathode was investigated.
- Both Sb and Bi contributed the capacity by forming solid intermetallics with Li.
- The Li‖Sb-Bi cell exhibits a high energy efficiency of 89%.
- The cost of electrode materials in the Li‖Sb-Bi cell is 68 $ kWh^{-1}.

GRAPHICAL ABSTRACT

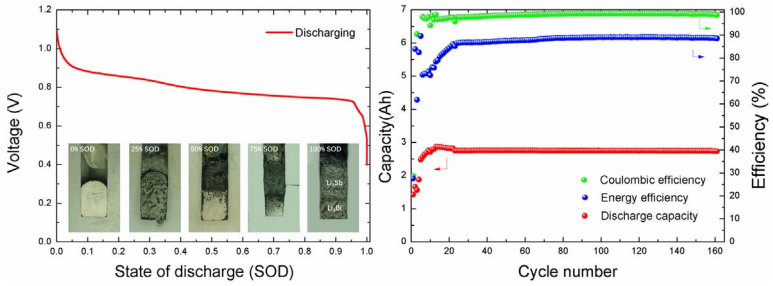

ARTICLE INFO

Keywords:
Liquid metal battery
Bismuth-antimony alloys
Cathode capacity
Energy storage

ABSTRACT

Li-Bi based liquid metal batteries (LMBs) have attracted interest due to their potential for solving grid scale energy storage problems. In this study, the feasibility of replacing the bismuth cathode with a bismuth-antimony alloy cathode in lithium based LMBs is investigated. The influence of the Bi:Sb ratio on voltage characteristics is evaluated via the constant current discharge method and electrochemical titration. On observing the cross section of the electrode at various stages of discharge, it is determined that both Sb and Bi form solid intermetallics with Li on the cathode. Additionally, the addition of Bi not only reduces the melting temperature of the Bi:Sb intermetallic but also actively contributes to the electrode capacity. Thereafter, a Li|LiCl-LiF|Sb-Bi liquid metal battery with 3 A h nameplate capacity, assembled and cycled at 1 C rate, is found to possess a stable capacity for over 160 cycles. The overall performance of this battery is discussed in the context of cost effectiveness, energy and coulombic efficiencies.

1. Introduction

In an endeavor to reduce CO_2 emission, renewable energy technologies, such as wind and solar energies, are being integrated with the base load supply of the electric grid. However, to ensure continuous supply of electricity from the grid, the power generated from these renewable energy sources, which is quite intermittent, needs to be first stored in large-scale energy storage devices. Additionally, the storage devices should be robust enough to manage short-term fluctuations in both energy generation and demand. In that context, large-scale

* Corresponding author. Center for Advancing Materials Performance from the Nanoscale (CAMP-Nano), State Key Laboratory for Mechanical Behavior of Materials, Xi'an Jiaotong University, Xi'an 710049, PR China.
** Corresponding author.
E-mail addresses: xiaohuining@mail.xjtu.edu.cn (X.-H. Ning), liju@mit.edu (J. Li).

https://doi.org/10.1016/j.jpowsour.2018.01.048
Received 5 December 2017; Received in revised form 8 January 2018; Accepted 19 January 2018
Available online 08 February 2018
0378-7753/

stationary electric energy storage (SEES) devices, like rechargeable batteries, can fulfill this dual role of integrating renewable energy sources and improving the grid reliability by offering spatial and temporal flexibility in electric energy management. The temporal flexibility originates from a battery's ability to charge and discharge whenever required, while the convenience involved in storing it at the supply end (such as a power station) as well as the consumer end (like a housing estate) contributes to its spatial flexibility. Due to these merits, batteries were initially considered as ideal candidates for short-term and mid-term stationary electricity storage [1,2]. However, since they are relatively expensive, have a short cycle life and are associated with multiple safety issues, their application in grid scale energy storage became uncommon [3–5].

Following the invention of liquid metal batteries (LMBs) by Prof. Donald R. Sadoway, most of the above mentioned problems have been resolved, leading to renewed interest in developing battery technologies [6,7]. Unlike the conventional "SLS" (solid-liquid-solid) battery, a typical LMB has a three-layer structure, consisting of two liquid metal electrodes and a molten salt electrolyte. Owing to density differences and mutual immiscibility, the electrolyte is typically sandwiched between the two liquid metal electrodes [6,8–12].

Extending the concept of an all liquid LMB, Ning et al. designed a self-healing Li-Bi liquid metal battery [13]. Here, the Li_3Bi intermetallic cathode, which is initially solid when the battery is in the discharged state, transforms to the liquid state upon attaining full charge. This solid-liquid transformation is distinct from the solid-solid transformation of most battery electrodes. Because the liquid state erases all microstructural "memory" and damage of the electrode, the capacity loss diminishes. However, the relatively low equilibrium voltage (~ 0.7 V at two-phase region) of Li‖Bi cell and the high energy cost of the Li-Bi electrode couple (240$ kWh^{-1}) [7] leave a lot of room for improvement. Alternatively, Wang et al. and Li et al. developed electrodes for LMBs from the Li-Sb-Pb alloy and Li-Sb-Sn alloy system, respectively [14,15]. Since Pb and Sn have low melting points, their alloys with Sb possess the optimum melting point for functioning as liquid cathodes in LMBs. Unfortunately, Pb and Sn do not enhance the cell capacity.

In this study, by extending the above-mentioned concept, we develop a novel LMB that utilizes Bi-Sb alloy as the cathode. The addition of Sb to Bi serves the following 3 purposes. First, much like Pb and Sn, Bi lowers the melting point of Sb and hence facilitates easy liquefaction of the electrode at operating temperatures. Second, since Sb is relatively inexpensive, by adjusting the mole fractions of Sb and Bi, the total cost of the Li‖Sb-Bi cell can also be reduced [7]. Finally, and most importantly, both Sb and Bi contribute to the overall cell capacity.

As expected, experimental results show that the addition of Sb to Bi enhanced the discharge voltage of the Li‖Sb-Bi cell as well as its capacity and the cyclic energy efficiency. Moreover, among the 4 alloys prepared in this study, by varying the mole fractions of Bi and Sb, it was found that the 60:40 mol % Bi-Sb alloy exhibits the highest discharge voltage. After examining the cross-section images of each of these alloys, it was determined that the discharging cycle resembles an extraction process, wherein antimony and bismuth forms intermetallics with lithium and separated into different layers. In addition, based on the schematic phase diagram of Li-Sb-Bi at 550 °C, the relationship of discharge voltage variation and the evolution of different phases were analyzed. Upon testing the cyclic performance of an assembled Li‖Sb-Bi cell, a round-trip energy efficiency of 89% was obtained. To the best of our knowledge, this is amongst the highest values of efficiencies ever reported for LMBs.

2. Experimental

2.1. Preparation of molten salts electrolyte

LiF and LiCl (99.99%, all from Aladdin) were mixed in the proportion of 69.6:30.4 mol% to prepare the eutectic LiF-LiCl electrolyte (T_m = 501 °C) [16]. To obtain an anhydrous and homogeneous form of the electrolyte, the LiF-LiCl mixture underwent the following treatment: (1) The mixture is heated at 80 °C for 20 h in vacuum; (2) It is then heated at 250 °C for 20 h in vacuum; (3) Thereafter, in an Argon gas atmosphere, the mix was further heated to 550 °C for 2 h; (4) The melt is then cooled to room-temperature in the same atmosphere, and transferred to a glove box. (5) Finally, the solidified electrolyte inside the glove box is ground to a powder [13].

2.2. The three-electrode set-up

In order to exclude the influences of anode (Li) during electrochemical testing, the three-electrode set-up was used to investigate the electrochemical performance of Bi-Sb alloys with different compositions. Also, to ensure that the Bi-Sb alloy remains in the liquid state at the operating temperature in the range of 450 °C–550 °C, depending on the melting point of electrolyte (like LiF-LiCl-LiBr, 443 °C [16]), 4 alloys with Bi:Sb ratios corresponding to 90:10 mol%, 80:20mol%, 70:30mol % and 60:40mol% are developed as four kinds of working electrodes (WEs), and are displayed in Fig. S1 and Fig. S2 (a) [17,18]. On the other hand, a 60:40 mol% Li-Bi alloy and a 40:60 mol% Li-Bi alloy served as the reference electrode (RE) and counter electrode (CE) respectively. As Fig. S2 (b) shown, the composition of reference electrode locates at the two-phase region at 550 °C to avoid the potential variation if the composition had a little change during the electrochemical testing, according the Gibbs phase rule. As for the counter electrode, it is important to contain as much as lithium at the premise of being liquid at the operating temperature, so as to minimize the polarization. High-purity tungsten wires with a diameter of 1 mm were used as leads for all the electrodes. Homogeneous Bi-Sb alloy electrodes were prepared by placing pre-weighed Bi and Sb inside BN (boron nitride) crucibles (inner diameter of crucibles ~ 5 mm) and heating them to 650 °C, followed by cooling to room temperature in Argon gas atmosphere. Based on the Li-Bi phase diagram (see Fig. S2 (b)), the reference electrode and the counter electrode were melted at 850 °C in a 5 mm-inner-diameter BN crucible and at 550 °C in a 20 mm-inner-diameter BN crucible, respectively. All the materials used, i.e. Li, Bi, Sb, and tungsten wires, had a purity of 99.999% and were procured from ALADDIN Reagent (Shanghai) Co., Ltd. An electrochemical workstation (CHI660E, *CHEN HUA, Shanghai*) was used to characterize the electrochemical cycling. The electrodes were prepared, assembled and tested in an Argon gas atmosphere.

2.3. Microstructure observations

The 80:20mol% and 60:40mol% Bi-Sb alloy electrodes in the three-electrode cell were discharged to different levels, or to different states of discharge (SODs), and then lifted out of the molten salts. Then, these electrodes were cooled and sealed with epoxy. In order to observe the microstructure of these Bi-Sb alloy electrodes at different SODs, the cross-sections of the cooled and sealed electrodes were cut and polished to a mirror finish. Field emission scanning electron microscope (SEM, Hitachi SU6600), energy-dispersive X-ray spectroscopy (EDS, EDAX) and X-ray diffraction (XRD, PANalytical X'pert Pro) were used to analyze the morphology, element distribution and phase structure of these cross-sections.

2.4. Cell assembly and testing

The 60:40mol% Bi-Sb alloy and pure lithium were used to assemble a two-electrode full cell with the theoretical capacity of 3 A h. The materials were used in proportions of 80:12:8mol% (Li:Bi:Sb), which means the lithium had an excessive capacity of 1 A h. First, we melt the pre-weighed Bi-Sb mix at 650 °C and then cool it to obtain a homogeneous 60:40mol% Bi-Sb solid alloy. Next, by placing a foam anode collector inside a liquid lithium pool, lithium metal was absorbed onto

the anode. Later, after the foam anode collector was cooled to the room temperature, by comparing the mass difference, we can calculate the amount of lithium in the anode. Thereafter, the mass of pre-melted Bi-Sb alloy cathode was determined and weighed according to the amount of lithium present in the anode. Next, the cathode and pre-melted LiF-LiCl electrolyte were kept inside the cathode container and heated to 550 °C, following which, the cathode and molten salts get liquefied and instantly stratify according to their densities. Finally, after immersing the foam anode collector into the molten electrolyte slowly, this cell was cooled and sealed. All these assembly processes were conducted inside an Ar-filled glove box (Unilab, MBraun). A battery tester (BT2000, Arbin) was used to conduct the galvanostatic charge-discharge performance test.

3. Results and discussion

Equal quantities of the 90:10 mol%, 80:20mol%, 70:30mol% and 60:40mol% Bi-Sb alloys were discharged at a current density of 50 mA cm^{-2} in the three-electrode cell to evaluate the influence of composition on the electrochemical properties of the electrode. Also, all the working electrodes had the same active area and all the electrical leads were of the same length, thus ensuring that all the ohmic polarization overpotentials, evaluated from kinetics at 50 mA cm^{-1} were the same. The actual compound potentials of the Bi-Sb alloys discharged at 50 mA cm^{-2} are presented in Fig. 1. It is obvious that all four electrodes exhibit the same discharge capacity, irrespective of the Bi-Sb ratio. In each of these discharging curves, a clear voltage enhancement section and a voltage plateau, at approximately ~0.8 V and ~0.65 V, are observed. Note that, the voltage enhancement section gets progressively extended with an increase in the mole fraction of Sb in the alloy, which might also manifest from some reaction or transformation pertaining to Sb. The average discharge voltages of the four WEs are listed in Table 1. Of these WEs, since the 60:40mol% Bi-Sb alloy exhibits the highest value of the average discharge voltage, it also discharges the maximum amount of energy compared to other compositions.

To exclude kinetic factors during discharging, the coulometric titration technique was used to obtain the equilibrium potential of this electrode during discharging. In this method, the composition of the 60:40mol% Bi-Sb alloy working electrode in the three-electrode cell is varied by electrochemically titrating lithium for 2500 s at a constant current density of 50 mA cm^{-2} while recording the electrode potential. Each titration step was followed by an open circuit measurement for 2500 s, which allows the electrode composition to homogenize. The measured equilibrium potential is displayed in Fig. 2 (a) and its variations are plotted as a function of the SOD in Fig. 2 (b). As can be seen from these figures, it is evident that the voltage enhancement section and the voltage plateau appear successively, at about 0.83 V and 0.7 V. Note that since pure bismuth also exhibits an equilibrium potential of 0.7 V at 550 °C, the observation of the voltage plateau in the potential curve of 60:40mol% Bi-Sb alloy (see Fig. 2 (b)) might be related to the former's presence [19].

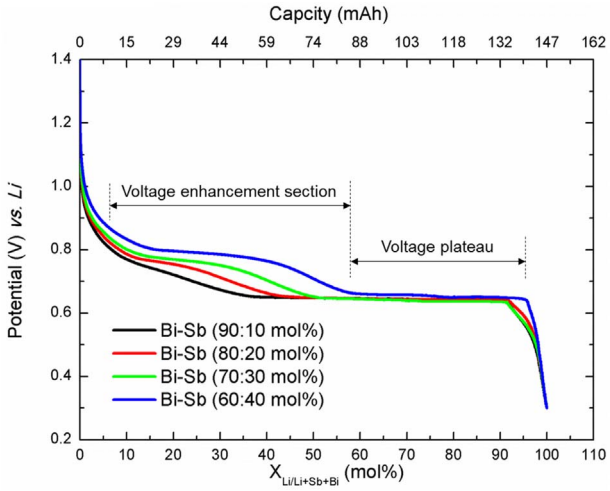

Fig. 1. The discharge curves of working electrodes in the three-electrode cell at the current density of 50 mA cm^{-2}.

Table 1
The average discharge potentials of different Bi-Sb alloy compositions.

Alloy Composition	Average discharge potential/V
Bi-Sb (90:10 mol%)	0.663
Bi-Sb (80:20 mol%)	0.667
Bi-Sb (70:30 mol%)	0.711
Bi-Sb (60:40 mol%)	0.734

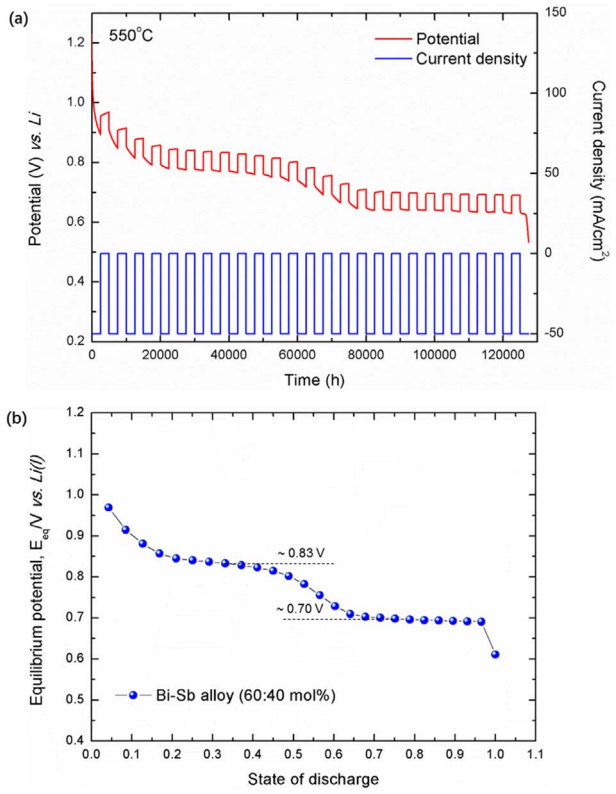

Fig. 2. (a) Potential and current curves of the coulometric titration of lithium into 60:40mol% Bi-Sb alloy working electrode at 550 °C with the 60:40 mol% Li-Bi alloy reference electrode and the 40:60 mol% Li-Bi alloy counter electrode (b) The equilibrium potential data as a function of 60:40mol% Bi-Sb alloy's state of discharge.

To understand the mechanism of the discharging process, the microstructures and phase evolution of Bi-Sb alloy electrodes in three-electrode cell were further investigated. For this, the cross section of 80:20mol% and 60:40mol% Bi-Sb alloy electrodes were characterized by SEM and XRD after quenching them at different discharge states.

Fig. 3 (a) displays the cross section optical and SEM images of the 80:20mol% Bi-Sb alloy, which was discharged by 10% (corresponding SOD ~ 0.1 or a capacity ~ 0.015 A h; Also see Fig. 1). Compared to the fully charged electrode (see Fig. S3 (a)), several newly formed millimeter sized particles can be seen on the electrode surface. Elemental analysis of these particles reveals the presence of Sb and O, while Bi was completely absent. It should be mentioned here that oxygen is incorporated in the electrode via lithium oxidation during electrode preparation. Therefore, the distribution of O in the EDS element mapping indirectly represents the distribution of Li in the particles [15]. When the electrode to further discharged by 40%, these dispersed solid

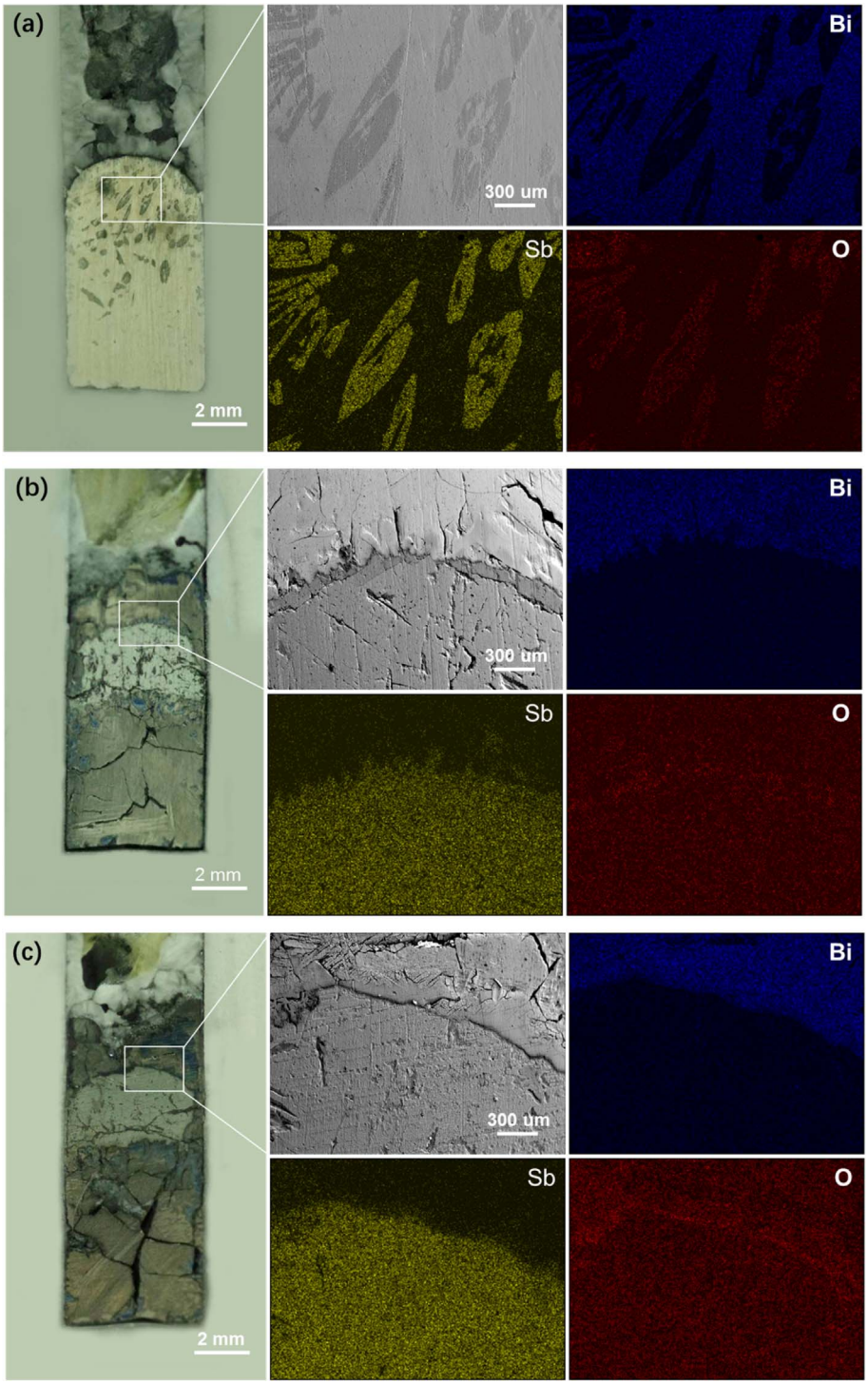

Fig. 3. The microstructure and elemental distribution in the cross section of 80:20mol% Bi-Sb alloy electrodes (a) after 10% discharge (b) after 40% discharge and (c) after getting fully discharged in the three-electrode cell.

phase particles accumulate into a continuous mass at the center of the electrode, with a clear interface separating it from the rest of the alloy (see Fig. 3 (b)). This continuous mass hardly grows further and the structural morphology of the electrode remains invariant even after full discharge (SOD ~1), as is evident from the optical micrograph displayed in Fig. 3 (c). Elemental analysis of the electrode in the fully discharged state reveals that of the three layers formed, the middle one primarily contains Sb, while the other two are rich in Bi. For the sake of convenience, these layers were categorized by two zones; zone A refers to the Sb rich middle layer whereas zone B represents the other two Bi rich layers. These two zones of the fully discharged electrode were further characterized by XRD and the results are shown in Fig. 4. On identifying the corresponding peaks in the XRD curves obtained from zone A and zone B, it was confirmed that the composition of the former and latter is Li_3Sb and Li_3Bi, respectively. An additional peak that appears in both the curves, originates from the SiO_2 substrate.

A similar systematic microscopic investigation was conducted the 60:40mol% Bi-Sb alloy at various levels of discharging. Much like the previous case of the 80:20mol% electrode, discrete particles of the Li-Sb intermetallic forms on the electrode, as the snapshot taken at 25%

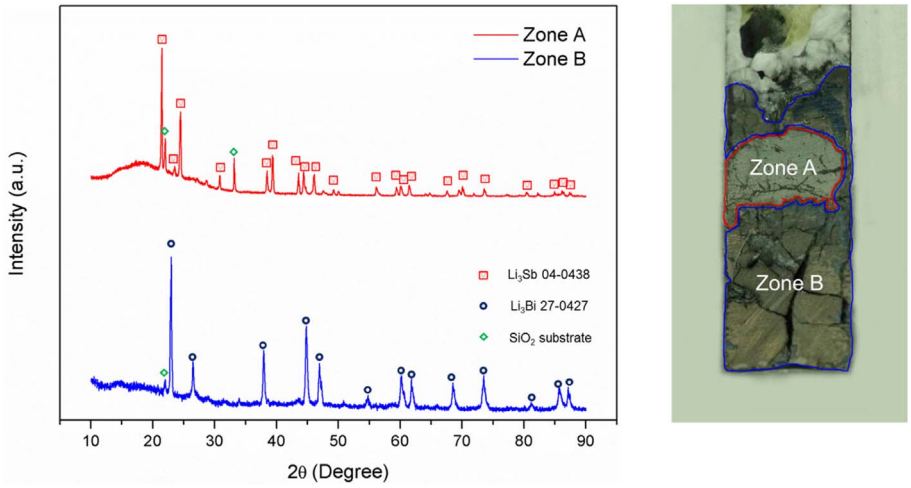

Fig. 4. The XRD results of the two zones on the cross section of a fully discharged 80:20mol% Bi-Sb alloy electrode in the three-electrode cell.

discharge indicates, (see and compare Fig. S3 (b) and Fig. 5). As shown in Fig. 5 (b)–(d), sustained discharging creates a continuous layer of the Li-Sb intermetallic, which is eventually separated from the adjoining Li-Bi layers by a clear phase boundary. Note that an additional snapshot at SOD ~0.75 is displayed in Fig. 5 (c) to illustrate the evolution of Li-Bi during the later stages of discharging. In fact, the progressive darkening– indicating Bi enrichment– of the lower portion of the cross-section shown in Fig. 5 (b)–(d), strongly validates the contribution of Bi to the occurrence of the voltage plateau in the discharge curves (See Fig. 1).

Based on these results, the discharging mechanism of the Bi-Sb alloy *vis-à-vis* the voltage variation can be described as follows. The onset of the voltage enhancement section in the discharging curve corresponds to consumption of Sb by Li to form the Li-Sb intermetallic. At a deeper level of discharging, Li starts combining with Bi to form Li_3Bi, which is responsible for the appearance of the voltage plateau. In some sense, the above-described discharging mechanism of the Bi-Sb alloy bears striking resemblance to a Sb extraction process, where Li separates Sb and Bi by alloying with it and segregates out as an individual phase having distinct boundaries. Additionally, since the final product contains Li_3Sb, in addition to Li_3Bi, it confirms that both Sb and Bi contribute to the overall capacity of the cell.

In Fig. 6 (a) a schematic illustration of the Li-Bi-Sb phase diagram[1] at 550 °C is displayed. Four different phase regions, labeled ①, ②, ③, ④ in the figure, correspond to the single-phase region (*Sb-Bi-Li liquid*), the 2-phase region (*Sb-Bi-Li liquid and Li_3Sb*), the 3-phase region (*Sb-Bi-Li liquid, Li_3Sb and Li_3Bi*) and the second 2-phase region (*Sb-Bi-Li liquid and Li_3Bi*), respectively. From this, the phase composition of different Bi-Sb alloys, depending on their state of discharge (or Li content), can be determined.

Since each alloy contains only Bi and Sb, their compositions, labeled with the corresponding percentages of Sb (10%, 20%, 30% and 40%), are marked on the Bi-Sb axis of the phase diagram. On discharging, the alloys absorb Li and their compositions progressively shift towards the vertex corresponding to Li. Dashed lines drawn from the initial compositions marked on the Bi-Sb axis to the Li vertex indicate the path over which alloys undergo compositional changes.[2] These composition paths have been constructed (using calculations in Ref. [20]) based on the data obtained from existing 2-phase phase diagrams (Li-Bi [18], Li-Sb [21], and Sb-Bi [17]). Note that regardless of the composition, each alloy transits through previously mentioned four phase regions in the Li-Bi-Sb ternary phase diagram. Using these paths as guidelines, the phase evolution of each Bi-Sb alloy on discharging is described as follows.

Initially, in the fully charged state, all the alloys exist in the form of liquid Sb-Bi-Li and are thus in the single-phase regime. Thereafter, on discharging, depending on the mole fraction of Sb in the Bi-Sb alloy, either of the two intermetallic phases, Li-Bi or Li-Sb, starts forming, and the alloy enters the two 2-phase region corresponding to ② or ④, respectively. In the previously conducted microscopic investigation, it was noted that both 60:40mol% and 80:20mol% Bi-Sb alloys first produce the Li-Sb phase, followed by the Li-Bi phase, on discharging. Therefore, it seems likely – looking at the Li-Sb-Bi phase diagram (see Fig. 6 (a)) – that the formation of the Li-Bi phase can precede that of the Li-Sb phase only if the initial mole fraction of Sb $<$ 20% in the Bi-Sb alloy. The exact critical point (purple color dot labeled 'A') separating the preferential occurrence of either phase corresponds to the intersection point of each phase boundary in the Li-Sb-Bi system and has been highlighted in Fig. 6 (a) for reference. Note that although, we have not specifically determined the sequence of phase formation in the 90:10mol% Bi-Sb alloy, we believe that the discharging-induced composition evolution path of a 90:10mol% Bi-Sb alloy will pass through the two phase region ④. With further discharging, the composition of all the alloys crosses the 3-phase region of the phase diagram, which consists of Li-Sb-Bi liquid along with the solid Li_3Sb and Li_3Bi phases. Finally, the alloys turn into a 2-phase mixture of solid Li_3Sb and Li_3Bi after full discharge.

In Fig. 6 (b), specific phase changes associated with different portions of the discharging curves for the 60:40 mol% and 90:10 mol% Bi-Sb alloy electrodes at 50 mA cm^{-2} are displayed. It should be mentioned that, the voltage drops much more rapidly in the liquid single-phase region than it does in others. This is because in this regime, the chemical potential is extremely sensitive to compositional changes of Sb, Bi and Li. As a result, after absorbing 23% of Li, the 90:10 mol% Bi-Sb alloy, which still exists in the liquid single phase regime, discharges to 0.7 V, whereas the 60:40 mol% Bi-Sb alloy, at the same discharge state, has a potential of 0.8 V.

Furthermore, the latter electrode discharges in a very stable fashion and retains a potential of 0.65 V even after absorbing ~60% Li, whereas the former discharges rapidly to the same voltage after absorbing just ~36% of Li. Finally, within the 3- phase regime ③, the potential no longer depends on the composition and both electrodes maintain a constant potential of 0.65 V (see Fig. 6 (b)). From these

[1] The ternary phase diagram in Fig. 6 (a) should only be used as a rough guide to understand phase evolution because although the distribution and composition of phase domains are accurate, the exact locations of the phase boundary lines are unknown.

[2] Note that the discharging process ends when the overall composition of each alloy reaches the 3-phase domain boundary that connects the Li-Bi and Li-Sb axes. The dashed lines have been further extended to the Li vertex only to indicate the direction along which the composition evolves on discharging.

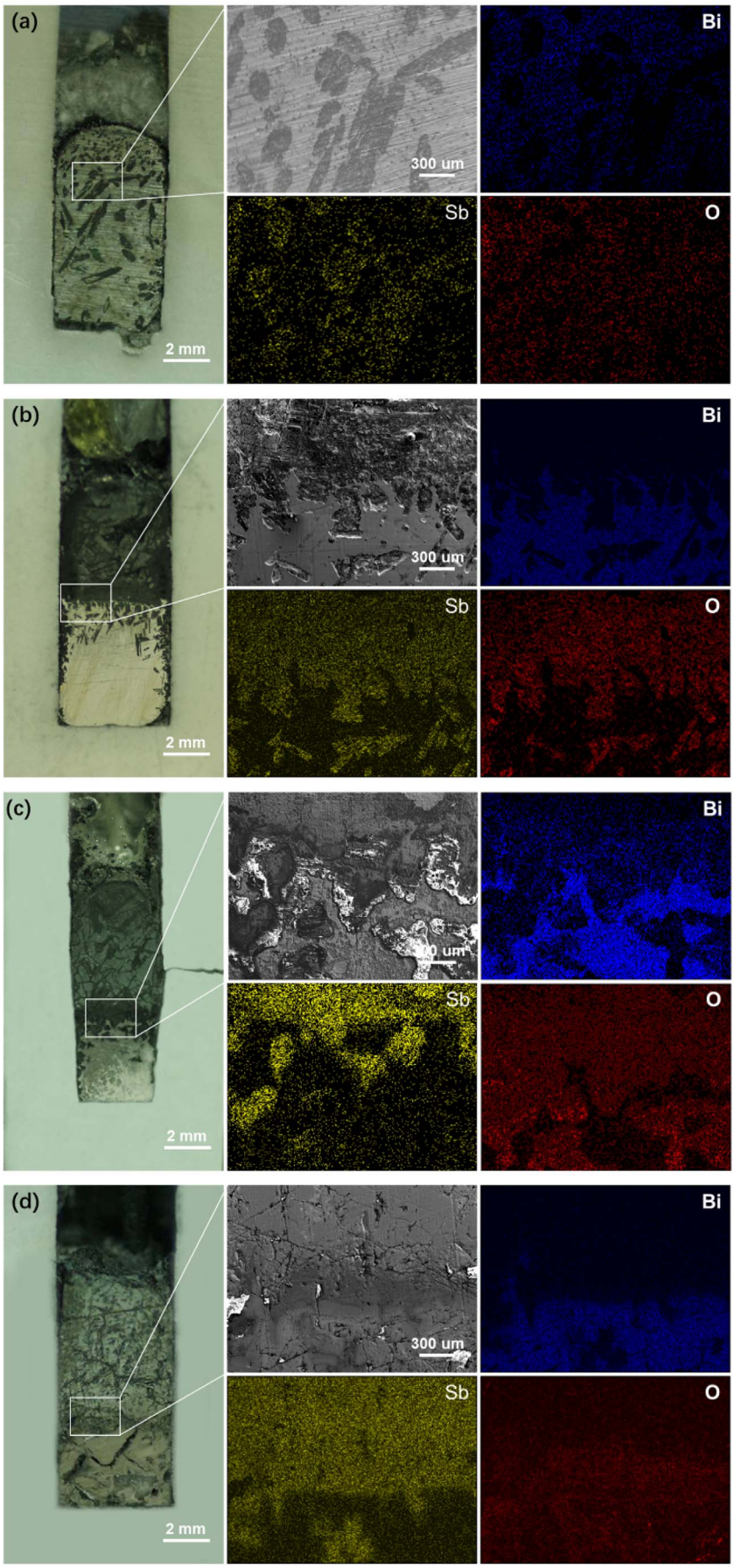

Fig. 5. The microstructure and elemental distribution in the cross section of the 60:40mol% Bi-Sb alloy electrodes (a) after 25% discharge (b) after 50% discharge (c) after 75% discharge and (d) after getting fully discharged in the three-electrode cell.

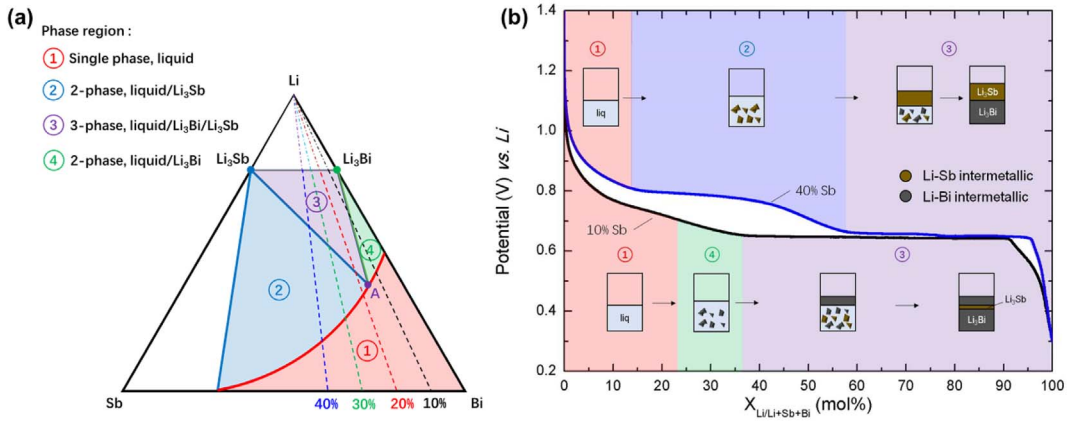

Fig. 6. (a) The estimated ternary phase diagram of Li-Sb-Bi alloy at 550 °C overlaid with lines depicting the composition profiles of different Bi-Sb alloys during discharging. (b) Evolution of different phases in the 60:40mol% Bi-Sb and 90:10mol% Bi-Sb alloys during discharging in the three-electrode cell.

observations, it is apparent that incorporating a higher mole% of Sb in the electrode promotes the formation of the Li-Sb phase ahead of Li-Bi phase. This expedites the transition of an electrode from the liquid single phase region to the 2-phase region (see Fig. 6 (a)), which in turn mitigates the drop in its potential during discharging. However, it is also not advisable to drastically reduce the spacial extent of the liquid single-phase region by adding increasing amounts of Sb, as this will compromise the ability of the electrode to self-heal.

An additional consequence of Li_3Sb forming ahead of Li_3Bi due to the increased content of Sb in the alloy is that the stacking sequence of the intermetallic layers will also change (see schematic in Fig. 6 (b)). Such a change in the structural configuration will affect diffusion rates and potentially influence the electrode's rate performance.

Therefore, to critically evaluate the influence of high Sb content on the rate performance of Bi-Sb alloys, the 60:40mol% Bi-Sb alloy electrode with a theoretical capacity of 147 mAh was discharged at different current densities ranging from 100 to 1000 mA cm^{-2}, in the three-electrode cell. From the discharge potential curves shown in Fig. 7, it is evident that the rate performance of the electrode is good and the cell approaches a theoretical capacity of ~150 mAh, at current densities lower than 400 mA cm^{-2}. However, when the current density is gradually increased beyond 400 mA cm^{-2}, the capacity rapidly diminishes and reduces to exactly half of the theoretical capacity at the current density of 1000 mA cm^{-2}. This capacity decline at higher current densities can be attributed to the progressive shortening of the lower potential plateau, which in turn suggests that the formation of Li-Bi intermetallics is getting suppressed. In comparison, a pure Bi electrode, by the virtue of having an extended single-phase liquid domain, facilitates rapid diffusion and hence exhibits superior rate performance [13]. However, considering the promotion of discharge voltage and energy density, the 60:40mol% Bi-Sb alloy cathode still serves as the best choice.

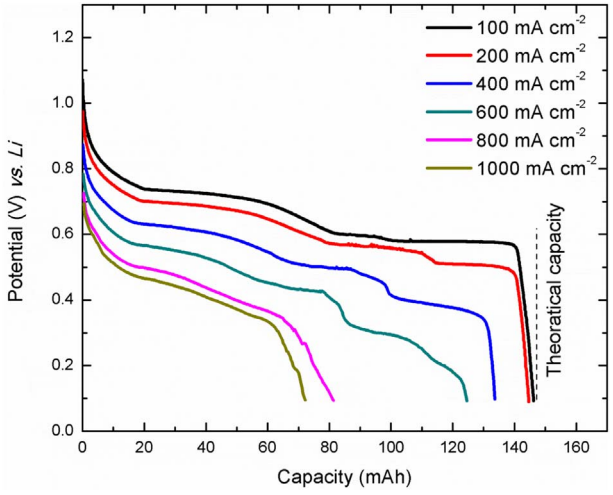

Fig. 7. The discharge potentials of 60:40mol% Bi-Sb alloy in the three-electrode cell at different current densities (range ~ 100–1000 mA cm^{-2}).

Finally, to investigate the cycling performance of a Li‖Sb-Bi cell, a typical two-electrode full cell with a 3 A h 60:40mol% Bi-Sb alloy cathode was assembled. Note that the anode (lithium) had an excessive capacity of 1 A h, which ensures a comprehensive electrochemical evaluation and the complete utilization of the Bi-Sb alloy. Fig. 8 (a) shows the charging and discharging curves in the 100 cycle of the cell at a current density of 150 mA cm^{-2}. The voltage enhancement section and the voltage plateau both can be seen on the curves. Furthermore, this cell exhibits excellent cycling performance with an overall energy efficiency of 89%, coulombic efficiency of 99% and cathode utilization of 91.67%, as shown in Fig. 8 (b). Compared to the Li‖Bi cell, the higher energy efficiency of the Li‖Sb-Bi cell originates from the addition of antimony to bismuth; as mentioned earlier, antimony would also contribute to the overall capacity of the cell. In terms of cost per unit energy, the cost of the latter is only 68 $ kWh^{-1}– a value comparable to that of Li‖Sb-Pb and Li‖Sb-Sn batteries – whereas the Li‖Bi cell costs 169 $ kWh^{-1} (See Table S1) [13–15].

Thus, with a superior capacity, the Li-Bi-Sb alloy is the best candidate for developing grid-scale liquid metal batteries.

4. Conclusion

In summary, under the premise of that the Bi-Sb alloy remains in the liquid state, 4 alloys with Bi:Sb ratios corresponding to 90:10 mol%, 80:20mol%, 70:30mol% and 60:40mol% were investigated for their potential use as cathodes for LMBs. Of these, the 60:40mol% Bi-Sb alloy was found to be the most desirable composition as it exhibits the highest average discharge voltage. Microstructural changes and the evolution of different phases in the 60:40mol% and 80:20mol Bi-Sb alloys at different SODs show that the solid Li_3Sb and Li_3Bi intermetallics are the final discharge products in Bi-Sb alloy electrodes, and the extraction of Sb by Li to form the Li-Sb intermetallic manifests as the voltage enhancement section in the discharge potential curves of these alloys. Besides, based on the schematic phase diagram, the relationship of discharge voltage and the phases evolution was analyzed, and we propose that the discharge rate performance of Bi-Sb alloy (60:40mol%) was slightly weakened by the reduction of liquid single-phase region because of the increasing amounts of Sb.

Furthermore, since Bi also transforms to the solid state by reacting with Li, the capacity of the electrode gets highly enhanced. There are several indications that just like the pure bismuth cathode, the Bi-Sb

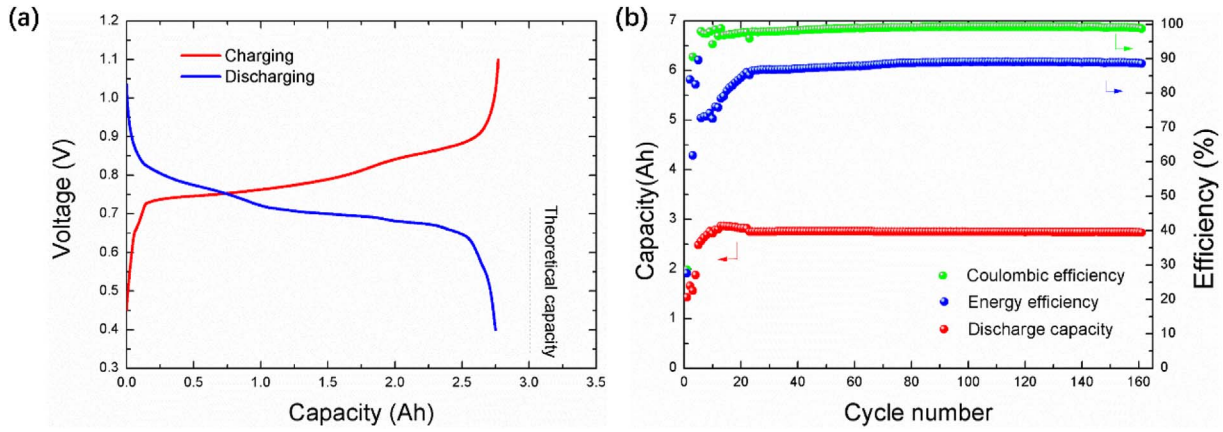

Fig. 8. The cycling performance of a Li||Sb−Bi cell at a current density of 150 mA cm^{-2} (a) Voltage profiles of the 100st cycle and (b) Discharge capacity, coulombic efficiency, and energy efficiency as a function of the number of cycles.

cathode can also heal itself by charging to the fully charged state. One of prerequisite is that the charging rate should be much slower than the self-healing rate, namely the alloying rate of liquid Bi with solid Sb. However, a more detailed study on this aspect needs to be conducted in future.

Finally, the performance assessment of a Li‖Sb-Bi cell reveals that it is better than many of the conventionally used alternatives in terms of overall energy, coulombic and cathode utilization efficiencies. These observations encourage future research on developing cathode materials for LMBs which will deliver better performance at lower cost.

Acknowledgements

This work was supported by the grants from National Natural Science Foundation of China (U1766216, 51401157) and Basic Science Research in Shaan Xi (2015JQ5164). JL acknowledges support by NSF DMR-1410636.

Appendix A. Supplementary data

Supplementary data related to this article can be found at http://dx.doi.org/10.1016/j.jpowsour.2018.01.048.

References

[1] B. Dunn, H. Kamath, J.-M. Tarascon, Science 334 (2011) 928–935.
[2] G.L. Soloveichik, Annu. Rev. Chem. Biomol. Eng. 2 (2011) 503–527.
[3] C. Wadia, P. Albertus, V. Srinivasan, J. Power Sources 196 (2011) 1593–1598.
[4] Z. Yang, J. Zhang, M.C. Kintner-Meyer, X. Lu, D. Choi, J.P. Lemmon, J. Liu, Chem. Rev. 111 (2011) 3577–3613.
[5] C.J. Barnhart, S.M. Benson, Energy Environ. Sci. 6 (2013) 1083.
[6] D.J. Bradwell, H. Kim, A.H. Sirk, D.R. Sadoway, J. Am. Chem. Soc. 134 (2012) 1895–1897.
[7] H. Kim, D.A. Boysen, J.M. Newhouse, B.L. Spatocco, B. Chung, P.J. Burke, D.J. Bradwell, K. Jiang, A.A. Tomaszowska, K. Wang, W. Wei, L.A. Ortiz, S.A. Barriga, S.M. Poizeau, D.R. Sadoway, Chem. Rev. 113 (2013) 2075–2099.
[8] H. Li, H. Yin, K. Wang, S. Cheng, K. Jiang, D.R. Sadoway, Adv. Energy Mater. 6 (2016) 1600483.
[9] S. Poizeau, H. Kim, J.M. Newhouse, B.L. Spatocco, D.R. Sadoway, Electrochim. Acta 76 (2012) 8–15.
[10] H. Kim, D.A. Boysen, T. Ouchi, D.R. Sadoway, J. Power Sources 241 (2013) 239–248.
[11] T. Ouchi, H. Kim, B.L. Spatocco, D.R. Sadoway, Nat. Commun. 7 (2016) 10999.
[12] T. Ouchi, D.R. Sadoway, J. Power Sources 357 (2017) 158–163.
[13] X. Ning, S. Phadke, B. Chung, H. Yin, P. Burke, D.R. Sadoway, J. Power Sources 275 (2015) 370–376.
[14] K. Wang, K. Jiang, B. Chung, T. Ouchi, P.J. Burke, D.A. Boysen, D.J. Bradwell, H. Kim, U. Muecke, D.R. Sadoway, Nature 514 (2014) 348–350.
[15] H. Li, K. Wang, S. Cheng, K. Jiang, ACS Appl. Mater. Interfaces 8 (2016) 12830–12835.
[16] P. Masset, R.A. Guidotti, J. Power Sources 164 (2007) 397–414.
[17] H. Okamoto, J. Phase Equil. Diffus. (2012) 1–2.
[18] W. Gasior, Z. Moser, W. Zakulski, Arch. Metall. 39 (1994) 355–369.
[19] W. Weppner, R. Huggins, J. Electrochem. Soc. 125 (1978) 7–14.
[20] The Materials Project Database. http://materialsproject.org.
[21] M.M. Kane, J.M. Newhouse, D.R. Sadoway, J. Electrochem. Soc. 162 (2014) A421–A425.